Effect of ponderomotive forces on wave dispersion and second-harmonic light emissions in laser-produced plasmas

S. Jackel, S. Eliezer, and A. Zigler
Plasma Physics Department, Soreq Nuclear Research Center, Yavne, Israel
(Received 27 October 1980)

In this paper we analyze the basic characteristics of experimentally observed second-harmonic light spectra generated during long-duration high-intensity laser-plasma interactions. It is shown that the observed spectrum characteristics of threshold, red-shift, and target material dependence can be explained by a two-step mechanism of parametric coupling affected by a strong "imposed" ponderomotive force. The imposed ponderomotive force, generated by the laser light's standing-wave pattern, affects the parametric coupling through increased linear wave dispersion. Experimental results agree with the theoretical prediction and suggest the existence of additional parametric instabilities in the ponderomotive-force-dominated regime.

I. INTRODUCTION

An important diagnostic used in the study of laser-plasma interactions is the light emitted at the second harmonic of the incident laser light's frequency. Spatially resolved measurements can yield information regarding the hydrodynamic evolution of the plasma[1,2] while spectrally resolved measurements can provide information regarding the mechanisms of laser light absorption near the critical density.[2-7]

Results obtained from experiments performed with long-duration laser pulses of low intensity (Nd:glass-$\lambda_{laser} = 1.06$ μm, $\tau_{laser} > 1$ nsec, $I_{laser} < 10^{15}$ W/cm^2 (Ref. 4); $CO_2 - \lambda_{laser} = 10.6$ μm, $\tau_{laser} > 10$ nsec, $I_{laser} < 10^{13}$ W/cm^2 (Ref. 5) have shown evidence consistent with the existence of parametric instabilities near the critical density. Experiments performed by us[6] and at Rutherford[7] have yielded data in the high-intensity long-duration regime (Nd:glass-$\lambda_{laser} = 1.06$ μm, $\tau_{laser} > 1$ nsec, $I_{laser} > 10^{15}$ W/cm^2). At these intensities the ponderomotive force, generated by the standing-wave pattern of laser light within the plasma, was believed to result in a steepening of the plasma's density profile and a turning off of the parametric instabilities.[8]

In this paper we show that instead of reduced instabilities, the data[6] suggest additional instabilities in the ponderomotive-force-dominated regime. In particular (Fig. 1), for intensities $\gtrsim 2 \times 10^{15}$ W/cm^2, an additional 2ω spectral component appears with the dominant characteristics of a parametric instability source: threshold, rapid growth rate, red shift, and red-shift dependence on target material (Z/A).

By including the effect of a strong imposed ponderomotive force on linear wave dispersion ("natural modes of the plasma"), we obtain expressions that accurately predict the measured 2ω red shifts. The strong imposed ponderomotive force is due to the laser light's standing-wave pattern within the plasma. Near critical density, where the 2ω light is generated, a resonant field structure may exist and the imposed ponderomotive force is of maximum strength. [Frequency shifts

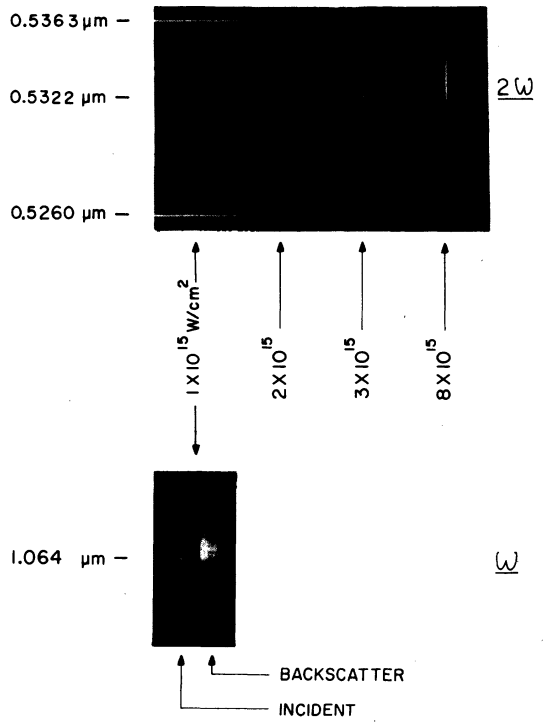

FIG. 1. 2ω and ω spectroscopic results for low-Z targets. The narrow lines superimposed on the 2ω spectra are calibration lines from a Rb vapor lamp. Incident and backscatter ω spectra were taken simultaneously. Bandwidth of the incident laser light is less than the 0.5-Å spectrometer resolution. The Brillouin-broadened and red-shifted ω spectra were not found to correlate with the 2ω spectra.

due to strong pump distortions (quasimodes) have been analyzed for Brillouin and Raman instabilities.[9] Some ω_0 backscatter spectra from laser-plasma experiments have been interpreted in terms of the existence of these quasimodes.[10]]

Our model also provides a possible answer to the question of why the parametric instabilities do not turn off as the density profile steepens. The model indicates the possibility of wave growth with energy extracted from the imposed ponderomotive force. This results in enhanced "noise levels" for those plasma waves of just the right frequencies to participate in the parametric coupling. Thus, both enhanced wave growth and enhanced convective dissipation occur at the same time.

The remainder of this paper is divided into three sections and two appendices. In Sec. II, the dispersion relations are derived for linear waves subjected to a strong imposed ponderomotive force. A normal mode analysis is used to derive the dispersion relations. In Sec. III, the dispersion relations together with the Manley-Rowe relations are used to derive the red shifts expected from a two-step parametric coupling process. We are here dealing with the parametric coupling of traveling waves within a background laser light-produced standing wave. (In general, the laser light forms a partial standing wave in the plasma. The standing wave is formed from that portion of the laser light which remains unabsorbed.) In Sec. IV, the experiment[6] is reviewed and the data are compared to the model predictions. The implications are then discussed. In Appendix A, we apply our model to the previously studied problem of Brillouin instability in the strong coupling regime.[9] We find that our model can also give reasonable agreement to the red-shift values calculated for the case of a strong traveling wave pump. In Appendix B we present a simple electronic analog of the plasma response to imposed ponderomotive forces.

II. WAVE PROPAGATION

Ponderomotive forces produced by focusing laser light in a plasma are believed to result in a number of effects: axial steepening of the density profile,[11] transverse profile modification with laser beam self-focusing,[12] and density rippling with turbulence production.[13] Wave propagation may be affected by the alteration of the density profile.[14]

Imposed ponderomotive forces may directly affect plasma-wave propagation through the dispersion of longitudinal-wave-induced density perturbations. This is similar to the action of plasma pressure in a hot plasma. Ponderomotive forces may also act as a source of energy for resonant plasma waves. This is a case of parametric amplification in which a time varying feedback signal in a resonant system modulates an otherwise dc source. (An electronic analogy is presented in Appendix B.)

To see in detail the effect of ponderomotive forces, note that the force per electron $\vec{f}'$ due to spatial variations of the imposed electric field $\vec{E}=\vec{E}_s(\vec{r})\cos\omega_0 t$ is given by[15]:

$$\vec{f}' = -\frac{1}{2n_{cr}}\vec{\nabla}\left(\frac{E_s^2}{8\pi}\right) + \frac{1}{8\pi n_{cr}}\left[\vec{\nabla}\left(\frac{E_s^2}{2}\right) - 2\vec{E}_s\times(\vec{\nabla}\times\vec{E}_s)\right]\cos 2\omega_0 t, \tag{1}$$

where n_{cr} is the critical density. The ponderomotive force is, in general, treated as a time-averaged quantity. Since, however, we are dealing with the interaction of the ponderomotive force with waves that may oscillate with frequencies up to $\omega\simeq\omega_0$, a time average is not appropriate.

The force exerted on a unit volume of plasma $\vec{F}$ is given by

$$\vec{F}=n\vec{f}', \tag{2}$$

where n is the electron number density. If a plasma wave of frequency ω passes through the region subjected to the imposed ponderomotive force $\vec{f}'$, then the electron density will vary as $n=n_0+n_1\cos\omega t$ and the ponderomotive force per unit volume will be given by

$$\vec{F} = -\frac{n_0}{2n_{cr}}\vec{\nabla}\left(\frac{E_s^2}{8\pi}\right) - \frac{n_1}{2n_{cr}}\vec{\nabla}\left(\frac{E_s^2}{8\pi}\right)\cos\omega t - \frac{n_0}{8\pi n_{cr}}\left[\vec{\nabla}\left(\frac{E_s^2}{2}\right) - 2\vec{E}_s\times(\vec{\nabla}\times\vec{E}_s)\right]\cos 2\omega_0 t - \frac{n_1}{8\pi n_{cr}}\left[\vec{\nabla}\left(\frac{E_s^2}{2}\right) - 2\vec{E}\times(\vec{\nabla}\times\vec{E}_s)\right]\cos 2\omega_0 t\cos\omega t. \tag{3}$$

Here, n_0 is the steady-state density and $n_1\cos\omega t$ is the induced density perturbation. In order to calculate the wave's dispersion relation, Eq. (3) [not just Eq. (1)] must be included in the electron momentum equation.

It is important to note that only the second term of Eq. (3) oscillates in unison with the density perturbing wave, and only it appears in the first-order expression defining the plasma's normal modes. The first term appears in the zeroth-order equation and is the cause of steady-state profile modification. The third term appears in the second-order equations and is a source term

for the current of frequency $2\omega_0$. Second-harmonic light generated by this current will not be red shifted and has been treated elsewhere.[16] The fourth term is equivalent to a higher-order plasma coupling with the driver at frequency $2\omega_0$, and remains non-resonant so long as $\omega \neq \omega_0$ or $\omega \neq 2\omega_0$. For the waves dealt with here, $\omega < \omega_0$ and the fourth term can be neglected.

In the remaining analysis only the component of the instantaneous ponderomotive force required for calculation of the linear dispersion relations will be retained. Defining $\vec{f}$ as the relevant component of $\vec{f}'$, we have that

$$\vec{f} \equiv -\frac{1}{2n_{cr}} \nabla \left(\frac{E_s^2}{8\pi}\right) = -\frac{1}{n_{cr}} \nabla \left\langle \frac{E^2}{8\pi} \right\rangle . \tag{4}$$

In Eq. (4) the equality $\langle E^2 \rangle = \frac{1}{2} E_s^2$ has been used. The quantity $\vec{f}$ is not, however, a time-averaged quantity.

The calculation of dispersion relations will be commenced with the treatment of Langmuir waves. Following Chen,[15] but including the term nf, the electron momentum, continuity, and Poisson's equation are given by

$$mn\left(\frac{\partial v}{\partial t} + v\frac{\partial v}{\partial x}\right) = -enE' - \frac{\partial p}{\partial x} + nf, \tag{5a}$$

$$\frac{\partial n}{\partial t} + \frac{\partial}{\partial x}(nv) = 0, \tag{5b}$$

$$\frac{\partial E'}{\partial x} = -4\pi en, \tag{5c}$$

where m and e are the mass and charge per electron, n, v, and p are the density, velocity, and pressure of the electrons, and E' is the induced electric field. It has been assumed that the problem is one-dimensional and that the ions are immobile. The high-frequency electron oscillations are adiabatic so that the equation of state is given by

$$pn^{-3} = \text{const.} \tag{6}$$

Linearizing about the steady state $n_0, v_0 = 0$ (n_0 may represent a point in the modified density profile) and assuming first-order variations of the form n_1, v_1, $E_1' \sim e^{i(kx-\omega t)}$, one obtains the system of first-order equations

$$-imn_0\omega v_1 = -en_0E_1' - i3k_BTkn_1 + fn_1, \tag{7a}$$

$$i\omega n_1 + in_0kv_1 = 0, \tag{7b}$$

$$ikE_1' = -4\pi en_1. \tag{7c}$$

The dispersion relation for Langmuir waves is obtained by combining (7a), (7b), and (7c). Thus,

$$\omega^2 = \omega_p^2 + \frac{3k_BT}{m}k^2 + \frac{if}{m}k, \tag{8}$$

where $\omega_p^2 = 4\pi e^2 n/m$.

Note in Eq. (8) the additional term that gives the ponderomotive force contribution to wave dispersion. The right-hand side is complex so that wave growth, fed by the imposed ponderomotive force, is possible. In the limit of $T \to 0$ (or when the imposed ponderomotive force dominates the plasma pressure), the real and imaginary parts of ω become

$$\omega_r = \left(\omega_p^2 + \frac{f^2k^2}{4m^2\omega_p^2}\right)^{1/2}, \tag{9a}$$

$$\omega_i = \frac{1}{2m}\frac{fk}{\omega_r}. \tag{9b}$$

It is of interest to note that when imposed ponderomotive forces are present, wave propagation occurs even for $T \to 0$. The amount of wave dispersion depends directly on the strength of the ponderomotive force. In the usual case of no imposed ponderomotive forces, the group velocity $(\partial\omega/\partial k)$ goes to zero as $T \to 0$ and wave propagation ceases. [Using Eq. (8) with $f = 0$, $T \to 0$.]

Ion-acoustic waves are next considered. The oscillation frequency is slow enough so that the ions and electrons move together. The electrons possess the system energy while the ions provide the inertia. The system response is specified by the electron momentum and continuity equations, the ion momentum equation, and an isothermal electron equation of state:

$$0 \simeq -en_eE' - \frac{\partial p_e}{\partial x} + n_ef, \tag{10a}$$

$$\frac{\partial n_e}{\partial t} + \frac{\partial}{\partial x}(n_ev_e) = 0, \tag{10b}$$

$$Mn_i\frac{\partial v_i}{\partial t} = eZn_iE', \tag{11c}$$

$$p_en_e^{-1} = \text{const.} \tag{10d}$$

Electron inertia has been neglected in (10a) and ion pressure has been neglected in (10c). Linearizing, assuming that $n_{i0} = Zn_{e0}$ (quasineutrality), and combining, as before, the dispersion relation for ion-acoustic waves is obtained:

$$\omega^2 = \frac{Z}{M}(k_BTk^2 + ifk). \tag{11}$$

M is the ion mass, Z is the ionization state, and T is the electron temperature. The real and imaginary part of ω in the limit of $T \to 0$ (or in the region where ponderomotive forces dominate over the plasma pressure) are

$$\omega_r = \left(\frac{1}{2}\frac{Z}{M}|fk|\right)^{1/2}, \tag{12a}$$

$$\omega_i = \frac{1}{2}\frac{Z}{M}\frac{fk}{\omega_r}. \tag{12b}$$

Here too, ion-acoustic waves can propagate even

for $T \to 0$.

The propagation of transverse electromagnetic waves is the last type to be considered. A TEM wave does not cause density oscillations so that $n_1 = 0$. (Electrons are caused to oscillate so that $v_1 \neq 0$.) The ponderomotive force $F' = nf'$ will not have an ω oscillatory component. Therefore, the ponderomotive force will not directly affect the dispersion relation for TEM waves. Its effect may, of course, be felt through an alteration of the zeroth-order density profile.[14]

At this point it is worthwhile to consider the imaginary parts of the dispersion relations, i.e., Eq. (9b) and (12b). Since n_1, v_1, and E_1 are proportional to $e^{-i\omega t} = e^{-i\omega_r t} e^{\omega_i t}$, growth of both Langmuir and ion-acoustic waves occurs for $\omega_i > 0$. From (9b) and (12b), this is seen to correspond to waves propagating out of the plasma. Inward propagating waves are damped and so do not build up out of any initially present noise.

Wave growth, by this mechanism, can occur only when and where there is the externally imposed ponderomotive force. Energy is taken from the ponderomotive force and is transferred to plasma waves. This may limit or damp the ponderomotive force.

III. 2ω SPECTRA

The production of 2ω light is a second-order effect resulting from either the second-order currents produced in conjunction with the resonant absorption process[16] or the parametric coalescence of plasma waves.[17] 2ω light generated via the second-order current of resonant absorption has a spectrum that is either centered on the $2\omega_0$ frequency or is blue shifted due to a plasma motion induced Doppler shift. 2ω light generated via parametric coalescence of plasma waves has a spectrum with a characteristic red shift. As was shown in previous work,[18] when the incident light intensity becomes strong enough, nonlinear effects alter the spectrum of 2ω light generated via parametric coalescence. As we will show, this nonlinear effect is just the additional wave dispersion induced by the imposed ponderomotive force.

2ω production via parametric coalescence is a two-step process. In the first step, the essential Langmuir wave is generated. This is generally thought to be the result of the parametric decay instability in which an incident laser light photon p decays into a plasmon (Langmuir wave) l, plus a phonon (ion-acoustic wave) i. (An alternate Langmuir wave production mechanism recently proposed by Cairns[19] involves coupling of the plasma oscillations generated in resonant absorption with ion-acoustic waves produced in heat flux instabilities.[20])

In the second step, a 2ω photon p' is produced through the coalescence of a plasmon and an incident light photon or through the coalescence of two plasmons. Schematically, these two steps can be represented by the relations

Step I.

$$p \to l + i, \tag{13a}$$

Step II.

$$l + p \to p', \quad l + l \to p'. \tag{13b}$$

Because the plasmon receives only part of the laser light photon's energy, it will, in step II, produce a 2ω photon with an energy less than $2\hbar\omega_0$ and with a frequency less than $2\omega_0$. This is the source of the 2ω spectrum's red shift.

The magnitude of the red shift is quantified by applying the Manley-Rowe relations to the parametric processes of steps I and II. Physically, the Manley-Rowe relations are just the conservation laws of momentum and energy applied to parametric wave coupling. For the wave coupling of step I:

$$p \to l + i \begin{cases} \vec{k}_0 = \vec{k}_1 + \vec{k}_2, & (14a) \\ \omega_0 = \omega_1 + \omega_2. & (14b) \end{cases}$$

For the wave coupling of step II:

$$p + l \to p' \begin{cases} \vec{k}_0 + \vec{k}_1 = \vec{k}_3, & (15a) \\ \omega_0 + \omega_1 = \omega_3, & (15b) \end{cases}$$

or

$$l + l \to p' \begin{cases} 2\vec{k}_1 = \vec{k}_3, & (16a) \\ 2\omega_1 = \omega_3. & (16b) \end{cases}$$

The subscript 0 represents the incident photon, 1 is the plasmon, 2 is the phonon, and 3 is the 2ω photon.

The wave vectors $k_0, \ldots, k_3$ can be eliminated through use of the dispersion relations (Sec. I). These are summarized below.

Incident light:

$$\omega_0^2 = \omega_p^2 + c^2 k_0^2, \tag{17a}$$

Langmuir wave:

$$\omega_1^2 = \omega_p^2 + 3\frac{k_B}{m} T k_1^2 + i\frac{f}{m} k_1, \tag{17b}$$

Ion-acoustic wave:

$$\omega_2^2 = \frac{Z}{M}(k_B T k_2^2 + i f k_2) \tag{17c}$$

2ω light;

$$\omega_3^2 = \omega_p^2 + c^2 k_3^2. \tag{17d}$$

In our experiment, a 1.064-μm wavelength diffraction-limited beam from a Nd:glass laser was used to irradiate gold and aluminum slab targets. The pulse duration was 2.5 nsec. Focused intensities up to 10^{16} W/cm^2 were achieved. 2ω spectra were obtained along with measurements of the corona temperature, ionization state, and the asymptotic plasma velocity.

Figure 1 shows 2ω spectra from Al targets for a series of shots with increasing laser intensity. At low intensities ($I_0 \lesssim 10^{15}$ W/cm^2), a single-peaked distribution is observed within several angstroms of $\lambda_0/2$. At a threshold of 2×10^{15} W/cm^2, 2ω light with a substantial red shift is observed. It first appears as a "pedestal" but then emerges as a distinct distribution. Its intensity increases rapidly until by 8×10^{15} W/cm^2 it has completely overpowered the original peak.

The red shift was found to be a function of Z/A. The measurements showed that for Al targets, $Z/A=\frac{1}{2}$ and the 2ω peak was red shifted by $\Delta\lambda = 11\pm3$ Å. For Au targets, $Z/A=\frac{1}{4}$ and $\Delta\lambda=5\pm2$ Å.

The 2ω component appearing at high intensities has the characteristics of a parametric instability source, i.e., threshold, rapid growth rate, 2ω red shift, and a red shift that is Z/A dependent. In order to compare the experimental and theoretical red shifts, the Doppler shift due to plasma expansion must be included. This shift is to the blue and is given by[23]:

$$\frac{\Delta\lambda_d}{\lambda'} \simeq \frac{2}{c}\left(\frac{Z}{M}k_BT\right)^{1/2}. \tag{23}$$

Using Eq. (23) we have that $\Delta\lambda_d \simeq 9$ Å for Al and $\Delta\lambda_d \simeq 7$ Å for Au ($T \simeq 1.5$ keV at 10^{16} W/cm^2). Adding these Doppler shifts to the experimental results yield the red shifts due to the parametric processes: $\Delta\lambda_p = 20$ Å for Al and $\Delta\lambda_p = 12$ Å for Au.

Referring back to Sec. III, it can be seen that these red shifts are much larger than can be accounted for by thermal dispersion. The red shifts are accurately predicted with the inclusion of the imposed ponderomotive force. From Eq. (22) we have for the $l+p$ and $l+l$ processes, respectively: $\Delta\lambda_p = 17, 25$ Å in Al and $\Delta\lambda_p = 12, 18$ Å in Au. The model prediction is, thus, quantitatively accurate.

In Sec. II it was shown how strong ponderomotive forces could increase wave dispersion. Since additional wave dispersion leads to the possibility of additional instabilities, the question arises of whether or not new or modified parametric instabilities exist in the high-intensity range. The 2ω data suggest that this may be the case. The observed threshold at 2×10^{15} W/cm^2 is also the intensity near which ponderomotive forces have been found to strongly affect other plasma processes.[24] The observed rapid growth above threshold suggests an instability increasing with intensity. Energy absorption measurements[25] indicate that, after losses due to stimulated backscatter are accounted for, some absorption mechanisms remain efficient at high intensities. Parametric instabilities may, thus, be contributing to the absorption of high-intensity, long-duration laser pulses.

To summarize, it has been shown that imposed ponderomotive forces affect plasma wave dispersion. This effect can be observed in the spectra of second-harmonic light emitted from laser-produced plasmas. The theoretical predictions agree with the experimental results. The data suggest additional parametric instabilities in the high-intensity region.

ACKNOWLEDGMENT

The authors wish to thank Steve Gitomer for his helpful discussions.

APPENDIX A

Brillouin backscatter has been previously studied in the strong coupling regime.[9] In these analyses there is no imposed ponderomotive force. There is an induced ponderomotive force caused by beating between the pump wave and the high-frequency wave produced in the parametric decay process. This induced ponderomotive force drives the ion-acoustic wave which, when the pump becomes strong enough, need not be at the normal mode frequency.

In our analysis an imposed ponderomotive force interacts with density perturbing waves to alter the normal mode frequencies of these linear waves. The parametric coupling processes considered in Sec. III imply the existence of additional induced ponderomotive forces. The beat frequencies are, however, always at a normal mode frequency.

Although the two theoretical models describe two physically different situations, it is still possible to compare the model predictions. We do this by taking the ion-acoustic frequency given by Eq. (12a), an estimate for the pondermotive force f which is compatible with the analysis of Forslund *et al.*[9] and the wave vector matching condition $k=2k_0$. To start, consider incident and reflected waves of the form $E_I = E_i e^{i(k_0x-\omega_0t)}$ and $E_R = E_r e^{i(k_rx-\omega_rt)}$. The total electric field is given by $E_T = E_I + E_R$. The ponderomotive force is given by Eq. (4) so that, with the assumption that ω_0

The red shift is calculated by combining the Manley-Rowe relation for the first-order process (14a) and (14b) with the Manley-Rowe relations for one of the two second-order processes (15a), and (15b) or (16a) and (16b), and with the real parts of the dispersion relations (17a)–(17d). In an inhomogeneous plasma, a solution is obtained with the assumption that the first- and second-order processes occur at the same point in space, i.e., at the same density.

To see the effect of the imposed ponderomotive force on the 2ω spectra, it is sufficient to consider the two limits of $f \to 0$ and $T \to 0$. The derivation, consisting of algebraic manipulation and the elimination of small terms, will not be presented. We only note that if the ion-acoustic wave has a frequency $\omega_2 \equiv \Delta\omega$, then the Langmuir wave will be red shifted by an amount $\Delta\omega$ to a frequency $\omega_1 = \omega_0 - \Delta\omega$. The 2ω light will be red shifted, depending on whether the coupling is $l+p$ or $l+l$, to a frequency $\omega_3 = 2\omega_0 - \Delta\omega$ or $\omega_3 = 2\omega_0 - 2\Delta\omega$. The 2ω light's wavelength shift is given by $\Delta\lambda' = \frac{1}{4}(\Delta\omega/\omega_0)\lambda_0$. In addition, by combining (12a) and (12b) with (15a)–(15c), it can be shown that the Langmuir wave source density n_s is given by $n_s/n_{cr} \simeq 1 - 2\Delta\omega/\omega_0$.

For the limit $f \to 0$ (plasma pressure dominates):

$$\frac{\Delta\lambda'}{\lambda'} \simeq \left((8\times10^{-7})\frac{Z}{A}T\right)^{1/2}, \quad p+l\to p', \quad l+l\to p'. \tag{18}$$

T is the electron temperature in keV, Z is the ionization state, and A is the atomic number.

For the limit of $T \to 0$ (ponderomotive forces dominate):

$$\frac{\Delta\lambda'}{\lambda'} \simeq \left|23\alpha\frac{Z}{A}\lambda_0 f\right|^{1/2}, \tag{19a}$$

$$\alpha = \begin{cases} 1, & p+l\to p' \\ 2, & l+l\to p'. \end{cases} \tag{19b}$$

f is in units of dyn/cm^3 and λ_0 is in units of cm. [Note that Eq. (18) is identical to the first term of the expression giving $\Delta\lambda$ as calculated by Krokhin.[18] Equation (19) is functionally similar to the second term in Krokhin's expression which, however, is written in terms of the incident laser light intensity.]

In order to obtain a numerical estimate for $\Delta\lambda'$ it is necessary to estimate the magnitude of the ponderomotive force. We do this by making use of Ginzburg's formulas for the field structure near the critical density.[21] Near the critical density there is a resonance between p-polarized light and the plasma. The maximum electric field E_{max} and the width of the resonant region ΔZ are given by

$$E_{max} \simeq \frac{1.2\omega_0}{\nu}\left(\frac{c}{2\pi\omega_0 l}\right)^{1/2} E_0, \tag{20a}$$

$$\Delta Z \simeq \frac{\nu}{\omega_0} l. \tag{20b}$$

ν is the effective collision frequency, l is the plasma density scale length, and E_0 is the light's electric field outside of the plasma. The ponderomotive force is given by

$$f = \frac{1}{n_{cr}}\nabla\left\langle\frac{E^2}{8\pi}\right\rangle \simeq \frac{1}{n_{cr}}\frac{E_{max}^2}{8\pi\Delta Z}. \tag{21}$$

By inserting Eqs. (21), (20a), and (20b) into Eq. (19a), an estimate of $\Delta\lambda'$ in the limit of strong ponderomotive forces is obtained:

$$\frac{\Delta\lambda'}{\lambda'} \simeq (5.3\times10^{-13})\left[\alpha\frac{Z}{A}\left(\frac{\lambda_0}{l}\right)^2\left(\frac{\omega}{\nu}\right)^3 I_0\right]^{1/2}. \tag{22}$$

I_0 is the incident laser light intensity in W/cm^2.

Numerical estimates can now be calculated. For $I_0 = 10^{16}$ W/cm^2 at $\lambda_0 = 1.06$ μm on an Al target: $Z/A = \frac{1}{2}$, $T \simeq 1.5$ keV,[6] $l/\lambda_0 \simeq 1$.[11] From numerical simulation, $\nu/\omega \simeq 0.05$.[22] Under these conditions, $\Delta\lambda' = 4$ Å from Eq. (18) for the thermal contribution and $\Delta\lambda' = 17$ Å ($l+p$), 25 Å ($l+l$) from Eq. (22) for the ponderomotive contribution. Clearly, the 2ω red shift due to the imposed ponderomotive force dominates the red shift due to thermal dispersion.

Before concluding this section, it should be pointed out that the above estimate passes an important consistency test, i.e., that the ponderomotive force is, in fact, large at the source location of the 2ω light. To see this, note that for a linear density profile $n/n_{cr} = 1 - Z/l$. Using (20b), the density at the edge of the resonance zone is given by $n_r/n_{cr} = 1 - \nu/\omega$. For $\nu/\omega \simeq 0.05$, $n_r/n_{cr} \simeq 0.95$. The 2ω source density can be shown to be approximately given by $n_s/n_{cr} \simeq 1 - 2\Delta\omega/\omega_0 \simeq 1 - 8\Delta\lambda'/\lambda_0$. For $\Delta\lambda'/\lambda_0 \simeq 1.6\times10^{-3}$, $n_s/n_{cr} \simeq 0.99$. The 2ω source is, thus, in the region of strong ponderomotive forces.

IV. DISCUSSION

An experiment was conducted by us[6] in which laser-produced plasmas were generated under conditions simultaneously favorable to parametric instabilities and ponderomotive forces, i.e., with long-duration high-intensity pulses. A similar experiment with similar results was performed at Rutherford.[7] We shall summarize only the important points.

$-\omega_r \ll \omega_0$, we have that

$$f \simeq -\frac{(k_0 - k_r)}{4\pi n_{cr}} \times \sin[(k_0 - k_r)x - (\omega_0 - \omega_r)t] E_i E_r \, .$$

Taking the maximum local value for f, using the condition that $k_r \simeq -k_0$, and that far above threshold $E_r \simeq E_i$,

$$f \simeq -\frac{k_0 E_i^2}{2\pi n_{cr}} \, . \tag{A1}$$

The ion-acoustic wave's frequency is obtained by inserting Eq. (A1) into Eq. (12a), setting $k = 2k_0$, and using the definitions for the ion plasma frequency ($\omega_{pi}^2 = \omega_{pe}^2 Zm/M$) and the quiver velocity [$v_{osc} = eE_i/(m\omega_0)$].

$$\frac{\omega_r}{\omega_0} = \sqrt{2}\,\frac{\omega_{pi}}{\omega_{pe}}\,\frac{v_{osc}}{c} \, . \tag{A2}$$

From Forslund *et al.*[9] we have that the quasimode frequency ω_q is given by

$$\frac{\omega_q}{\omega_0} = \frac{1}{2}\left(\frac{\omega_{pi}}{\omega_0}\,\frac{v_{osc}}{c}\right)^{2/3} \, . \tag{A3}$$

Although (A2) and (A3) differ somewhat, they give similar values for the ion-acoustic wave's frequency. At $n/n_{cr} = 0.1$: $\omega_r/\omega_q = 0.57$, 0.72, and 1.23 at $v_{osc}/c = 0.05$, 0.10, and 0.50, respectively. Thus, with an estimate for the ponderomotive force, reasonable agreement between the two models is obtained.

APPENDIX B

As with many plasma phenomena, there exists an analogy between the plasma response to imposed ponderomotive forces and an electronic circuit. In this section an analog circuit will be developed with characteristics similar to dispersion in Langmuir waves via an imposed ponderomotive force.

To form the analog circuit we start by noting that a plasma oscillation represents a normal mode of the plasma. This behavior is identical to the response of an LC circuit (inductor and capacitor linked in parallel) connected to an oscillatory current source j (see Fig. 2). In order

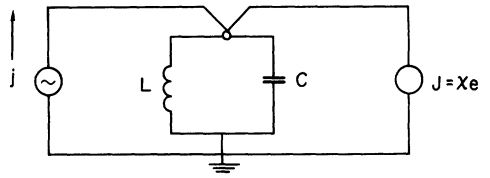

FIG. 2. An electronic analog to Langmuir waves in the high-intensity region. The response of the LC circuit to the oscillating source j is analogous to the plasma's response to Langmuir waves. The addition of the linear feedback controlled current source J, shifts the system's natural frequency and acts as an energy source just as occurs with strong imposed ponderomotive forces.

to introduce the ponderomotive force's analog, a second current source J is added in parallel to the LC circuit. The output of this current source is controlled by a feedback mechanism such that the current J is proportional to the voltage differential across the LC circuit, i.e., $J = \chi e$. As we will show, the current source J will shift the natural frequency of the circuit and that at resonance, J will add energy to the system.

The circuit equation for this system is

$$j + J = C\frac{de}{dt} + \frac{1}{L}\int e\,dt \, . \tag{B1}$$

Taking the Fourier transform and solving for e:

$$e = \frac{j}{-i(C\omega - 1/L\omega) - \chi} \, . \tag{B2}$$

The natural frequency is found by setting the denominator of Eq. (B2) equal to zero. Since the denominator is complex, ω will have real and imaginary parts. The growth rate γ is equal to ω_i.

$$\omega_r^2 = \frac{1}{LC} - \frac{\chi^2}{4C^2} \, , \tag{B3a}$$

$$\gamma = \frac{\chi}{2C} \, . \tag{B3b}$$

We thus see that the natural frequency ($\omega_p^2 \rightarrow 1/LC$) has been shifted by the introduction of the second current source ($F \rightarrow J$). The oscillation grows at a rate proportional to the gain of the second current source ($f \rightarrow \chi$) and inversely proportional to the system inertia ($m \rightarrow c$).

[1] A. Saleres, M. Decroisette, and C. Pataou, Opt. Commun. 13, 321 (1975); S. Jackel, J. Albritton, and E. Goldman, Phys. Rev. Lett. 35, 514 (1975); S. Jackel, B. Perry, and M. Lubin, *ibid.* 37, 95 (1976); J. Tarvin, Bull. Am. Phys. Soc. 25, 857 (1980).

[2] E. McClean, J. Stamper, B. Ripin, H. Griem, J. McMahon, and S. Bodner, Appl. Phys. Lett. 31, 825 (1977).

[3]J. Bobin, M. De Croisette, B. Meyer, and Y. Vitel, Phys. Rev. Lett. 30, 594 (1973); P. Lee, D. Giovanielli, R. Godwin, and G. McCall, Appl. Phys. Lett. 24, 406 (1974); C. Yamanaka, T. Yamanaka, T. Sasaki, J. Mizui, and H. Kang, Phys. Rev. Lett. 32, 1038 (1974).

[4]O. Krokhin, V. Pustovalov, A. Rupasov, V. Silin, G. Sklizkov, A. Starodub, V. Tikhonchuk, and A. Shikanov, Zh. Eksp. Teor. Fiz. Pis'ma Red. 22, 47 (1975) [JETP Lett. 22, 21 (1975)].

[5]C. Garban, E. Fabre, C. Stenz, C. Popovics, J. Virmont, and F. Amiranoff, J. Phys. (Paris) 39, L-165 (1978).

[6]S. Jackel, H. M. Loebenstein, A. Zigler, H. Zmora, and S. Zweigenbaum, Appl. Phys. Lett. 36, 34 (1980).

[7]D. Gray, J. Murdoch, S. Sim, A. Cole, R. Evans, and W. Toner, Plasma Phys. 22, 967 (1980).

[8]K. Lee, D. Forslund, J. Kindel, and E. Lindman, Phys. Fluids 20, 51 (1977).

[9]C. Liu, M. Rosenbluth, and R. White, Phys. Fluids 17, 1211 (1974); D. Forslund, J. Kindel, and E. Lindman, Phys. Fluids 18, 1002 (1975).

[10]R. Turner and L. Goldman, Phys. Rev. Lett. 44, 400 (1980).

[11]R. Fedosejevs, I. Tomov, N. Burnett, G. Enright, and M. Richardson, Phys. Rev. Lett. 39, 932 (1977); D. Atwood, D. Sweeney, J. Auerbach, and P. Lee, Phys. Rev. Lett. 40, 184 (1978); A. Raven and O. Willi, *ibid.* 43, 278 (1979).

[12]T. Donaldson and J. Spalding, Phys. Rev. Lett. 36, 467 (1976); M. Siegrist, Opt. Commun. 16, 402 (1976); C. Randall and J. De Groot, Phys. Rev. Lett. 42, 179 (1979).

[13]K. Estabrook, Phys. Fluids 19, 1733 (1976); B. Ripin, Appl. Phys. Lett. 30, 134 (1977).

[14]M. Sodha, G. Umesh, and R. Sharma, J. Appl. Phys. 50, 4678 (1979); M. Sodha, J. Sharma, D. Tewari, R. Sharma, and S. Kaushik, Plasma Phys. 20, 825 (1978).

[15]F. Chen, *Introduction to Plasma Physics* (Plenum, New York, 1974).

[16]A. Vinogradov and V. Pustovalov, Zh. Eksp. Teor. Fiz. 63, 940 (1972) [Sov. Phys.—JETP 36, 492 (1973)].

[17]V. Silin, *Parametric Action of High Power Radiation on a Plasma* (Nauka, Moscow, 1973).

[18]O. Krokhin, V. Pustovalov, A. Rupasov, V. Silin, G. Sklizkov, A. Starodub, V. Tikhonchuk, and A. Shikanov, Zh. Eksp. Teor. Fiz. Pis'ma Red. 22, 47 (1975) [JETP Lett. 22, 21 (1975)].

[19]R. Cairns, J. Plasma Phys. 22, 149 (1979).

[20]W. Manheimer and H. Klein, Phys. Fluids 18, 1299 (1975).

[21]V. Ginzburg, *The Propagation of Electromagnetic Waves in Plasmas* (Pergamon, New York, 1970).

[22]K. Estabrook, E. Valeo, and W. Kruer, Phys. Fluids 18, 1151 (1975); J. De Groot, C. Barnes, A. Walstead, and O. Buneman, Phys. Rev. Lett. 38, 1283 (1977).

[23]H. Kunze, in *Plasma Diagnostics*, edited by W. Lochte-Holtgreven (North-Holland, Amsterdam, 1968).

[24]D. Forslund, J. Kindel, and K. Lee, Phys. Rev. Lett. 39, 284 (1977); J. Kieffer, H. Pepin, F. Martin, P. Church, T. Johnston, and R. Decoste, Phys. Rev. Lett. 44, 1128 (1980).

[25]B. Arad, S. Eliezer, Y. Gazit, S. Jackel, Y. Karmi, H. Loebenstein, and A. Zigler, Appl. Phys. Lett. 37, 774 (1980).

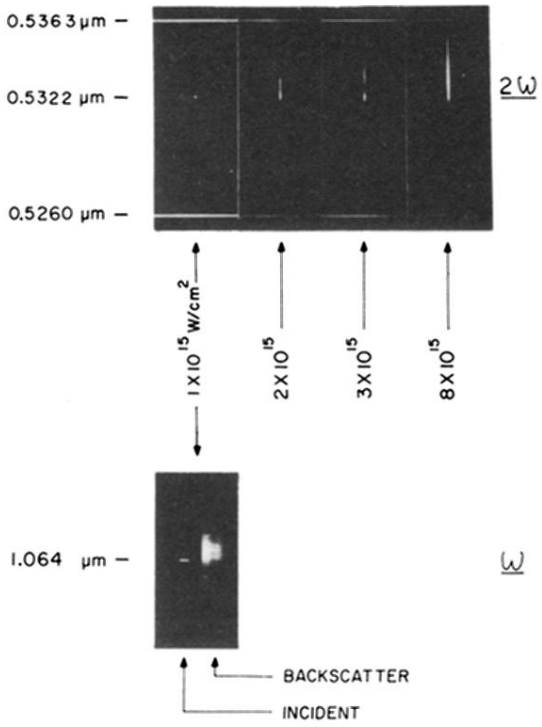

FIG. 1. 2ω and ω spectroscopic results for low-Z targets. The narrow lines superimposed on the 2ω spectra are calibration lines from a Rb vapor lamp. Incident and backscatter ω spectra were taken simultaneously. Bandwidth of the incident laser light is less than the 0.5-Å spectrometer resolution. The Brillouin-broadened and red-shifted ω spectra were not found to correlate with the 2ω spectra.